

Supramolecular hydrogel biomaterials and water-channels of differing diameters from dipeptide isomers

O. Bellotto[†], E. Scarel[†], G. Pierri[‡], P. Rozhin[†], S. Kralj^{§,‡}, M. Polentarutti[¥], A. Bandiera[¶], B. Rossi[¥], C. Tedesco^{‡*}, and S. Marchesan^{†,*}.

[†] *University of Trieste, Chem. Pharm. Sc. Dept., Via Giorgieri 1, 34127 Trieste, Italy.*

[‡] *University of Salerno, Chemistry & Biology Dept., Via Giovanni Paolo II 132, 84084 Fisciano (SA), Italy*

[§] *Jožef Stefan Institute, Materials Synthesis Dept., Jamova 39, 1000 Ljubljana, Slovenia*

[‡] *University of Ljubljana, Pharmaceutical Technology Dept., Faculty of Pharmacy, Aškerčeva 7, 1000 Ljubljana, Slovenia*

^{||} *Area Science Park, Padriciano 99, 34149 Trieste, Italy*

[¥] *Elettra-Sincrotrone Trieste, S.S. 114 km 163.5, Basovizza, 34149 Trieste, Italy*

[¶] *University of Trieste, Life Sciences Dept., Vian L. Giorgieri 5, 34127 Trieste, Italy*

^{*} *Corresponding authors. ctedesco@unisa.it; smarchesan@units.it*

KEYWORDS. Hydrogels; self-assembly; peptides; chirality; biomaterials.

ABSTRACT. Dipeptides stereoisomers and regioisomers composed of norleucine (Nle) and phenylalanine (Phe) self-assemble into hydrogels in physiological conditions that are suitable for cell culture. The supramolecular behavior, however, differs as the packing modes comprise amphipathic layers, or water channels, whose diameter is defined by either four or six dipeptide molecules. A variety of spectroscopy, microscopy, and synchrotron-radiation based techniques unveil fine details of intermolecular interactions that pinpoint the relationship between chemical structure and ability to form supramolecular architectures that define soft biomaterials.

Introduction

Hydrogels offer ideal environments for biomedical applications, as they provide mechanical support, hydration, viscoelastic properties that are ideally suited to mimic natural tissues and for biocompatibility, as well as the ability to encapsulate and deliver bioactive compounds.¹ Various biomolecular classes can be used as building blocks for promising performance, such as carbohydrates,²⁻⁵ proteins,⁶⁻⁷ and polypeptides.⁸⁻⁹ In particular, self-assembling peptide amphiphiles,¹⁰⁻¹³ and N-capped¹⁴⁻¹⁵ or uncapped¹⁶⁻¹⁹ short sequences have attracted researchers' attention for their ease of preparation and ability to fine control their purity and homogeneity, relative to macromolecular gelators of natural origin. Considering that the shorter is a peptide sequence, the lower will be its cost and ease of production, dipeptides stand out as an attractive option, as demonstrated by the well-known Phe-Phe motif,²⁰ and variations thereof.²¹⁻²³ Furthermore, the inclusion of non-proteogenic D-enantiomers and amino acids with non-natural side chains, such as norleucine (Nle), are attractive strategies to increase peptides' stability in biological environments and to fine-tune their supramolecular behavior. In this work, we show that all possible combinations of Nle and Phe in dipeptides lead to hydrogels that are compatible

with cell culture conditions, albeit the supramolecular packing, hence the resulting viscoelastic properties, varies greatly between isomers. The resulting assemblies encompass amphipathic layers and water-channels of varying diameters as they are defined by 4 or 6 dipeptide molecules. This is in marked contrast with Phe-Phe stereoisomers that consistently form water channels defined by 6 peptide molecules,²⁴ or Leu-Phe and Phe-Leu isomers, whose channels are defined by 4 peptides.²⁴ Furthermore, the use of synchrotron-radiation techniques allows to pinpoint key intermolecular interactions that are crucial for self-assembly.

Experimental Section

Materials and General Methods

All chemicals and solvents were purchased from Merck, except for 2-chlorotriyl chloride resin that was acquired from GL Biochem (Shanghai, China). The ¹H and ¹³C NMR spectra were acquired at 400 and 100 MHz, respectively, on a Varian spectrometer, using deuterated solvents as indicated in the Supporting Information. The dipeptides were synthesized in solid phase using Fmoc-protection strategy, purified by reverse-phase HPLC (Agilent 1260), and visualized by microscopy, using standard protocols previously applied to similar dipeptides.²⁵ Cell culture on peptide hydrogels and MTT assays were performed using standard protocols that have been previously described.²⁵

Self-Assembly Protocol

Peptides **1-4** were dissolved at the desired concentration (20-40 mM) in phosphate-buffered saline solution (PBS, 0.1 M) by heating the glass vial in an oil bath at 90 °C for 15-20 min. Upon cooling

down to room temperature, peptides **1-4** formed gels, and, in particular, the gel formed by peptide **4** displayed a metastable character as it converted into crystals within 2 hours.

Transmission electron microscopy (TEM)

TEM micrographs were acquired on Jeol, JEM 2100, Japan, at 100 kV. TEM grids (200 mesh copper-grid-supported carbon only and lacey carbon film, SPI, West Chester, USA) were treated for 20 min in a UV-ozone cleaner (UV-Ozone Procleaner Plus) to make the grids hydrophilic. After 1h of self-assembly, sample aliquots (~20 μ L) were deposited on top of a copper grid for 30 s. Next, water was drawn from the sample and the grid was placed for 30 s in contact onto a drop of 2% aqueous potassium phosphotungstate at pH 7.2. Finally, the grid was dried first at room temperature, and then *in vacuo*. Image analysis was performed using ImageJ software.

Crystallization

Compound **2** was dissolved in 50 μ l of dimethylsulfoxide (DMSO) to reach the final concentration of 98 mM. Then, 1 μ l of NaOH 1M was added to the clear solution. After few minutes, long needle crystals started to grow. Compounds **1**, **3**, and **4** crystallized spontaneously from the self-assembly test after several days.

Oscillatory Rheology

Hydrogels of compounds **1-3** were freshly prepared as described above (40 mM) and quickly transferred onto the bottom steel plate (flat, parallel geometry) of a Kinexus Plus rheometer (Malvern). Data were acquired at 25 °C (Peltier), using a 20-mm flat, top plate, and 1 mm gap. Frequency ramps were performed at 1 Pa, and stress ramps at 1 Hz. Each sample was prepared and

measured at least three times and representative measures are shown in the Supplementary Information.

Infrared and Visible Raman Spectroscopy

Samples were prepared as described above, and they were dried under vacuum overnight after being transferred either onto a 1-cm² piece of silicon wafer for attenuated total reflectance infrared (ATR-IR) spectroscopy, or onto a glass slide for visible Raman spectroscopy. ATR-IR spectra were recorded at 4 cm⁻¹ resolution, 240 scans, with IR Affinity-1S (Shimadzu). Raman spectra were registered using a 532 nm laser (5-10% power) with a Renishaw instrument. For each sample, spectra were recorded with 10-20 accumulations in several spots, using 1 cm⁻¹ resolution.

UV Resonance Raman (UVRR) spectroscopy

UVRR spectra were recorded using the multi-wavelengths UV Resonance Raman setup available at the BL10.2-IUVS beamline of Elettra Synchrotron Trieste (Italy). An excitation energy at 213 nm was set. All UVRR spectra were collected in back-scattered geometry by using a single pass of a Czerny-Turner spectrometer (Trivista 557, Princeton Instruments, 750 mm of focal length) equipped with a holographic grating at 1800g/mm and with a Peltier-cooled CCD camera. The resolution was set at about 1.3 cm⁻¹/pixel. The spectrometer was calibrated with cyclohexane (spectroscopic grade, Merck). Any possible photo-damage was avoided by continuously spinning the sample cell during spectra acquisition. All samples were freshly prepared as described above and placed in quartz cuvettes for UVRR measurements. A sample holder equipped with a thermal bath coupled to a resistive heating system was used to control the temperature of the samples during the measurements (temperature stability of ±0.1 K). The temperature was set at 298 K unless otherwise indicated in the text.

X-ray Crystallography

Single crystal X-ray diffraction. Single crystals of **1** (CCDC 2321385), **2** (CCDC 2321386), **3** (CCDC 2321387) and **4** (CCDC 2321388) were analyzed by single crystal X-ray diffraction. For each compound, a single crystal of suitable quality was collected with a loop, cryoprotected by dipping it in glycerol, and then frozen in liquid nitrogen for storage. Using the facility's robot, single crystals of **1**, **2** and **4** were measured at 100 K at XRD1 beamline (Elettra, Trieste, Italy), while **3** was measured at 100 K at XRD2 beamline (Elettra, Trieste, Italy). The rotating crystal method was used to collect diffraction data using synchrotron radiation with a wavelength 0.7000 Å for the data collected at XRD1 and 0.6199 Å for the data collected at the XRD2. For further details on the structure solution and refinement, see ESI. Mercury²⁶ was used as a crystal structure drawing tool. to draw Deposition Numbers CCDC 2321385-8 refer to the crystallographic data deposited at the Cambridge Crystallographic Data Centre (CCDC).

Powder X-ray diffraction. 1.0 boron glass capillaries filled with the corresponding solution of compounds **1-4** were left to dry overnight at room temperature in a vacuum chamber and then stored sealed. X-ray diffraction images were collected at 100 K at XRD1 beamline (Elettra, Trieste, Italy) by spinning the capillary using a wavelength of 0.7000 Å. The software FIT2D²⁷ was used to obtain experimental XRPD patterns from 2D diffraction images. Calculated XRPD profiles for all four crystal structures were obtained by using the software Mercury.²⁶

Circular Dichroism (CD) Spectroscopy

CD spectra were acquired on a Jasco J815 spectropolarimeter at 25 °C (Peltier), using 0.1 mm quartz cells, 1 s integration, stepsize of 0.5 nm, 1 nm bandwidth, and 25 accumulations. The

dipeptides were dissolved at 1 mM in milliQ water, and the pH was adjusted to 7.0 by adding NaOH (1 M) dropwise.

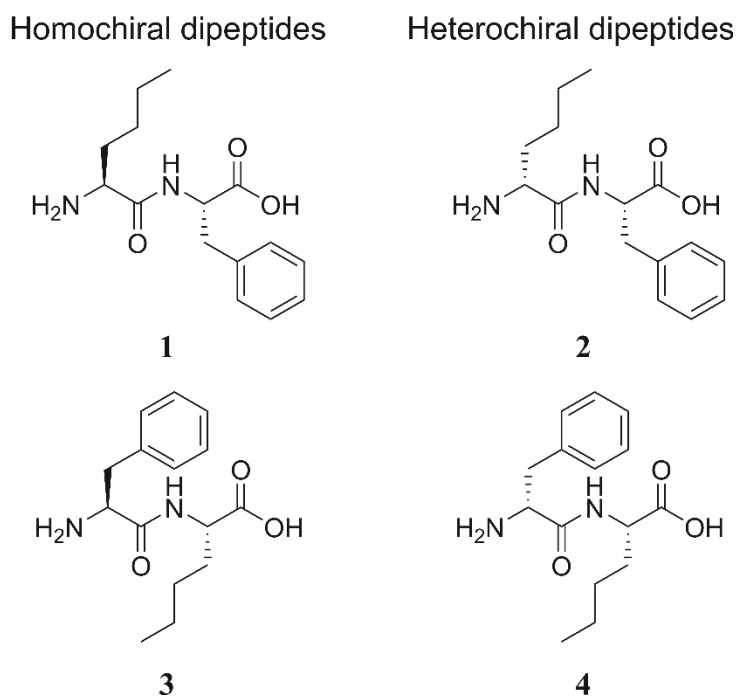
Results and Discussion

Gelation of dipeptides

There are 8 possible dipeptides arising from all possible combinations of Nle and Phe. Considering that enantiomers will display identical supramolecular behaviour in achiral environments, the 4 non-enantiomeric dipeptides shown in Scheme 1 are representative of the whole series. The 4 compounds were prepared by solid phase, purified by reversed-phase HPLC, freeze-dried, and their identity and purity were confirmed by LC-MS, ¹H-NMR, and ¹³C-NMR spectroscopy (see ESI, Sections S1-S4). The HPLC retention times (Table 1) can be considered an experimental measure of hydrophobicity, from which it was apparent that heterochirality significantly increased the hydrophobicity of the peptides, regardless of the sequence.

Nevertheless, all compounds gelled in phosphate-buffered saline (PBS) with minimum gelling concentrations (mgc) in the range of 20-30 mM, as shown in Table 1, although the gel of compound **4** was metastable and converted into crystals over 1 hour. Rheological analyses revealed that the sequences with Nle at the N-terminus (*i.e.*, **1** and **2**) formed stiffer gels than those with Phe at the N-terminus (*i.e.*, **3** and **4**), and that heterochiral **2** formed stiffer gels than the more hydrophilic homochiral counterpart **1** (Table 1 and ESI, Section S7). Stress sweeps revealed a linear viscoelastic range (LVR) up to 6 Pa for **1** and **2**, and up to 2 Pa for **3** (see ESI, Section S7). Finally, all gels were thermoreversible, with melting onset at 55 °C (40 mM), complete dissolution in the range 70-85 °C, and gelation occurring again when the samples were cooled down at room temperature (see ESI, Section S8). Overall, heterochirality and presence of Phe at the C-terminus

led to better gelling properties, analogously to dipeptides Leu-Phe and Phe-Leu.²⁸ Besides, presence of the linear Nle side chain, as opposed to the branched Leu regioisomer, favored self-assembly and reduced the mgc.²⁸ We inferred that the higher conformational flexibility of Nle side chain favored supramolecular packing, as noted for similar tripeptides.²⁹



Scheme 1. The four non-enantiomeric dipeptides **1-4**.

Dipeptide	Gel?	Gelation time ^a	Stable?	mgc (mM)	G' (Pa) ^a	HPLC Rt (min.)
1	Yes	2 min.	Yes	25	$1.4 \cdot 10^5$	11.8
2	Yes	2 min.	Yes	25	$2.2 \cdot 10^5$	13.1
3	Yes	5 min	Yes	30	$8.0 \cdot 10^4$	11.8
4	Yes	1 min.	No	20	n.a.	13.2

Table 1. Self-assembly into hydrogels of **1-4** dipeptides in PBS. ^agelator concentration of 40 mM.

Microscopy analysis of dipeptide nanostructures and microstructures

Electron and optical microscopy were used to investigate the ability of compounds **1-4** to self-assemble into nanostructures and microstructures, respectively. All isomers displayed remarkably similar behavior at the nanoscale, assembling into low-contrast thin fibrils that proved sensitive to electron beam irradiation damage, thus they were challenging to image by transmission electron microscopy (TEM). Fibril diameter measurements revealed multimodal distributions that were compatible with fibrils of 4-5 nm width that bundled together (Fig. 1). In particular, those from sample **4** (Fig. 1D) revealed a marked tendency to run parallel to each other in the same direction, as opposed to twist together into bundles.

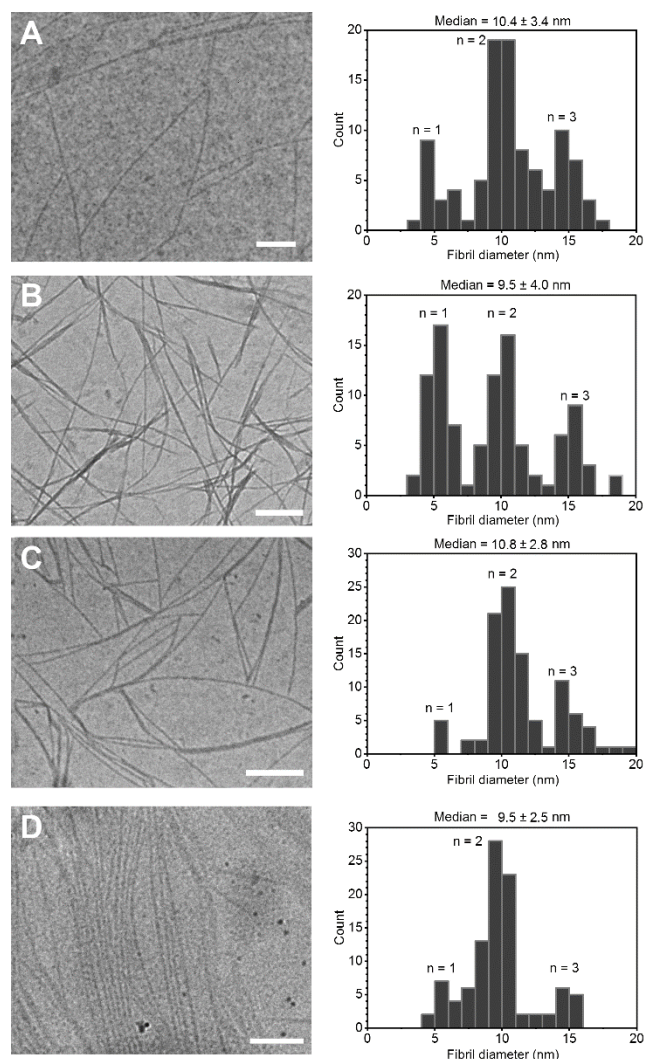


Figure 1. TEM images (left) and fibril diameter distribution (right, 100 counts) of compounds **1** (A), **2** (B), **3** (C), and **4** (D). Scale bars = 200 nm.

Interestingly, at the microscale, marked differences between the 4 isomers started to emerge. When observed under an optical microscope (Fig. 2), all samples displayed bundles of fibrils, although of increasing rigidity from **1** to **4**, with those from the latter being rapidly replaced by crystals, which allowed XRD analysis (*vide infra*). This observation was in agreement with the marked tendency of the fibrils of **4** to mutually interact as they oriented parallel to each other, as seen by TEM (Fig. 1D).

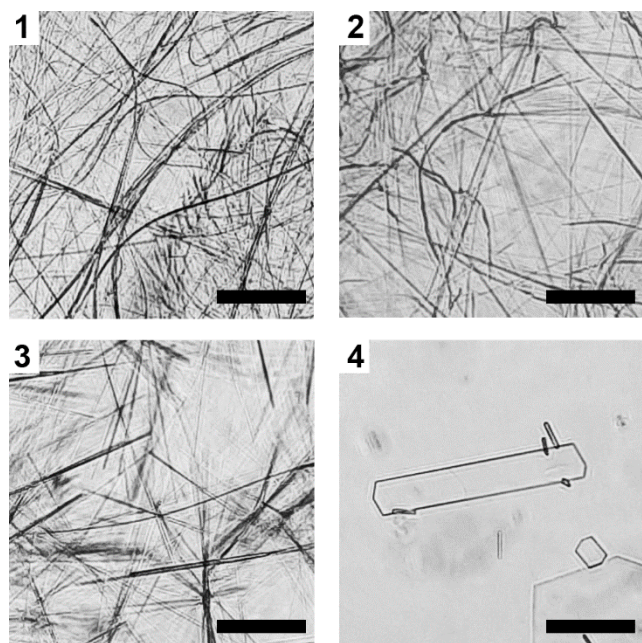


Figure 2. Optical microscopy images of compounds **1-4** in PBS. Scale bars = 100 microns.

Visible and UV Resonance Raman (UVRR) spectroscopies

Visible Raman spectroscopy is a useful technique that can provide insights into changes arising with self-assembly (Fig. 3). Microscopy image mapping of the fibers was possible only using the most intense Raman signal of the aromatic ring of Phe at $\sim 1003\text{ cm}^{-1}$ (yellow in the insets) that

was uniformly distributed along the fibers. Analysis with visible light of the powder and of the xerogels revealed the rising of specific signals (blue asterisks in Fig. 3) with self-assembly, except for compound **1** that displayed them already in the powder form (black asterisks in Fig. 3A-3B). In particular, they were at 742-744, 763-767, 782-786, 827-833, 867-873, 905, 946-948, 1155, 1197-1201, 1250-1255, 1400, and 1685-1688 cm^{-1} for compounds **1** and **3**. Assembly of compound **2** was also accompanied by the rising of peaks at 748, 836, 867, (903 already present in the powder), 952, (1156 already present in the powder), 1196, 1253, 1398, and 1689 cm^{-1} , suggesting a similar packing. Interestingly, D-Phe-L-Phe xerogel - but not the powder - also displayed characteristic peaks at 745, 867, 947, 1198, 1250, 1396, and 1684 cm^{-1} as it formed supramolecular water-channel whose cavities are defined by 6 dipeptide molecules.²⁴ In particular, the latter three signals fall in the amide I-III regions, and they are typically associated with the establishment of extended H-bonding networks in supramolecular dipeptide stacks.³⁰

By contrast, xerogels of compound **4** differed from the powder for peaks at 775, 811, 893, 927, 951, 970, 1095, 1107, 1130, 1247, 1278, 1312, 1345, 1415, 1542, 1558, and 1662 cm^{-1} . The wavenumbers differ considerably from the other three compounds, suggesting a different supramolecular packing.

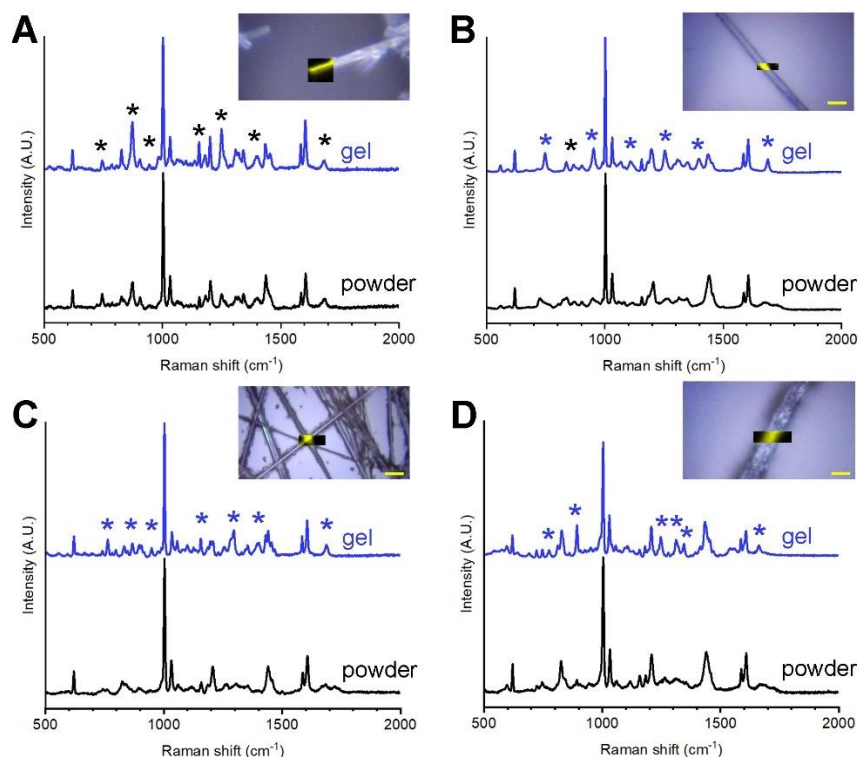


Figure 3. Visible Raman spectra and microscopy images with mapping at 1003 cm^{-1} (yellow in insets, scalebar = 10 microns) of compounds A) **1** B) **2** C) **3** D) **4** in the xerogel (blue) and powder (black) forms. Blue asterisks denote signals rising with assembly, in black when they were already present in the powder (in A).

Next, we employed UV resonance Raman (Fig. 4), which is a synchrotron-radiation technique that presents various advantages, when compared with conventional visible-light Raman spectroscopy. Firstly, it enables sample analyses both in solution and hydrogel phases, instead of xerogels whereby bulk water was removed. Secondly, it is possible to select the most appropriate excitation wavelength in the UV-range to enhance aromatic signals, such as those of the Phe benzene ring.³⁰ In this case, upon excitation at 213 nm, it was possible to observe that all **1-4** gels in their hydrated state displayed enhanced peaks at 1584 and 1604 cm^{-1} , corresponding to C-C stretching modes of the Phe side chain (Fig. 4A).³¹ In the case of compound **1**, it was possible to monitor the

crystallization process, acquiring spectra *in operando* whilst heating from 298 K to 372 K. The phase transformation was accompanied by sharpening of the aromatic signals and further rising of the peak at 1692 cm⁻¹ (Fig. 4B). This Raman mode corresponds to the amide I signal of the supramolecular state whereby the network of H-bonds is present already in the hydrated gel, and further extends during crystallization, confirming analogous packing modes in both states. Therefore, UVRR provided further evidence of the interactions holding together the supramolecular architecture in the hydrogel and in the crystal phases.

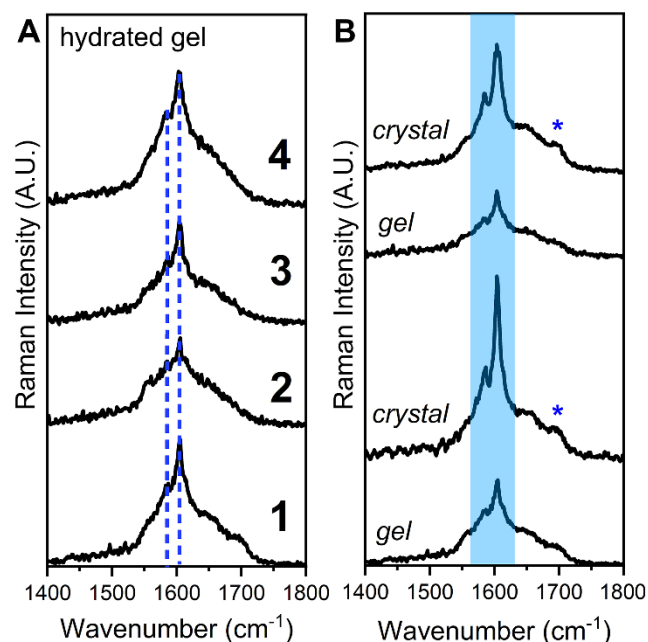


Figure 4. UVRR spectra. A) hydrogels 1-4. B) gel-crystal transition for 1.

Single-crystal and powder X-ray diffraction (XRD) analysis

Single crystals of suitable quality for X-ray diffraction (XRD) analysis were obtained from compounds 1, 3 and 4, under conditions that were very similar to the hydrogels, suggesting similar packing in the two phases, as supported by powder XRD data on xerogels. In particular, compounds 1 and 3 formed supramolecular water-channels, albeit with significantly differing

inner diameters (*i.e.*, 1.0 nm and 0.5 nm) as they were defined by 6 and 4 peptide molecules, respectively (Fig. 5). This is in marked contrast with analogs with Leu instead of Nle, which packed to form water-channels with a diameter defined by 4 peptide molecules, regardless of the order of amino acids along the sequence.³² Compound **1** crystallizes in a monoclinic system ($P2_1$ space group), while compound **3** in a tetragonal system ($P4_1$ space group). Interestingly, the asymmetric unit in crystal structure of **1** has three independent molecules with a pseudo-six-fold axis symmetry (see ESI Section S9 for details). Furthermore, because of highly disordered water molecules, we opted to use a solvent mask in the refinement procedure of **1**. The two crystal structures show the typical supramolecular arrangement of the Phe–Phe class described by Görbitz,³³ with the dipeptides arranged head-to-tail to define the hydrophilic water channels parallel to the shortest axis and the side chains segregated into the hydrophobic region. Furthermore, both structures share an H-bond pattern in which two amino H atoms interact with two carboxylic oxygen atoms of two distinct dipeptides, with the third interacting with a water molecule inside the channel. The latter interaction was proven in the case of compound **1** by studying a model in which the water molecules were not masked. Weak hydrophobic interactions established by the Phe and Nle side chains help to hold together the tubes through the establishment of steric zippers, which is a common feature for amyloids³⁴ that can stabilize hydrogels formed by hydrophobic short peptides with Leu and Phe.³⁵ Interestingly, not only replacement of Leu with Nle enables the formation of nanotubes with varying diameter, but also it enables formation of steric zippers that stabilize the hydrogel of **3**, while such a feature is absent in the analog Phe-Leu, which fails to gel under analogous conditions.²⁸

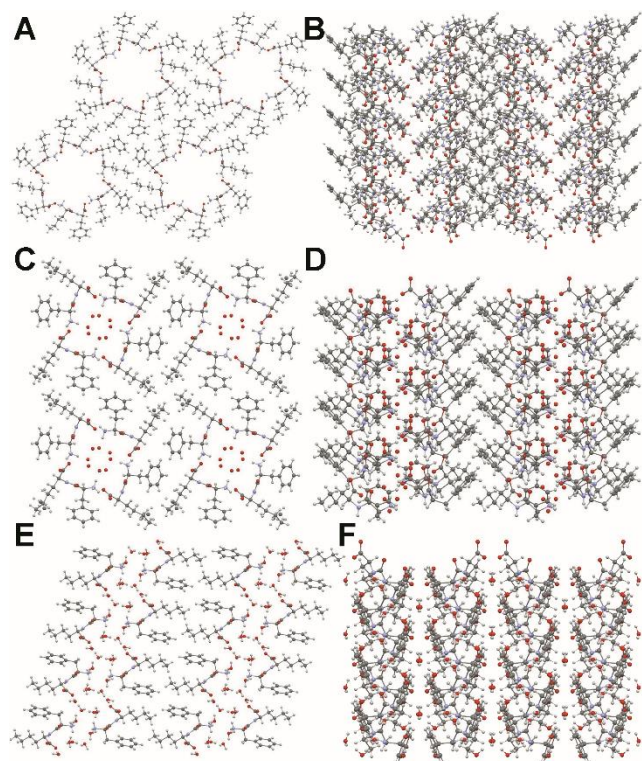


Figure 5. A-B) Crystal packing of L-Nle–L-Phe (**1**) (CCDC 2321385) along the *b* (A) and *c* (B) axes, respectively, disordered water molecules are not displayed. C-D) Crystal packing of L-Phe–L-Nle (**3**) (CCDC 2321387) along the *c* (C) and *a* (D) axes, respectively. E-F) Crystal packing of D-Phe–L-Nle (**4**) (CCDC 2321388) along the *b* (E) and *c* (F) axes, respectively. Only the atoms with the highest occupancy factors are shown.

A higher degree of similarity is instead found between heterochiral **4** and its analog with Leu instead of Nle,²⁸ as both displayed a metastable character with crystals arising from the hydrogel over time. The packing in both cases shows distinctive amphipathic layers within a monoclinic system (space group *C2*), with water layers parallel to the shortest *b* axis (Fig. 5E-F). The hydrophilic amide-rich region is formed by four dipeptides, whereas the side chains are gathered in the hydrophobic region forming weak interactions and excluding the water molecules. The disordered water molecules can be considered enclosed within channels and they create hydrogen

bonds with all three amide H atoms. Furthermore, also all the three carbonyl oxygen atoms form hydrogen bonds with the guest molecules. However, in marked contrast with the packing of compounds **1** and **3**, in the case of **4** the water channels are interconnected. The host-host interactions are mediated by the carbonyl oxygen atoms O1 and O3. In particular, carbonyl oxygen atom O1 interacts with the hydrogen atom of the phenyl ring ($C11 \cdots O1 = 3.401(1) \text{ \AA}$, $C11-H11 \cdots O1 = 2.49 \text{ \AA}$, $\angle C7-H7 \cdots O1 = 161.0^\circ$) while oxygen atom O3 interacts with the amide N-H atom ($N2 \cdots O3 = 2.853(1) \text{ \AA}$, $N2-H2 \cdots O3 = 2.01 \text{ \AA}$, $\angle N2-H2 \cdots O3 = 159.8^\circ$). These two interactions ensure the alignment of the dipeptides along the *b* axis.

Finally, crystals of suitable quality for XRD structural elucidation were obtained for compound **2** only in a mixture of DMSO and water, after numerous attempts. The layered structure of **2** is defined by two interconnected channels enclosed by hydrophobic side chains parallel to the shortest unit cell axis *c* and filled with DMSO, resembling the crystal packing of the dipeptide L-Leu-D-Ile (Fig. 6). While the third hydrogen atom of the $-NH_3^+$ directly interacts with the DMSO molecule located inside the channel ($N1 \cdots O1S = 2.8749(8) \text{ \AA}$, $N1-H1B \cdots O1S = 2.00(5) \text{ \AA}$, $\angle N1-H1B \cdots O1S = 161(4)^\circ$), the other two interact head-to-tail with the $^-OOC-$ group to define the layered structure ($N1 \cdots O3 = 2.756(1) \text{ \AA}$, $N1-H1A \cdots O3 = 1.94(3) \text{ \AA}$, $\angle N1-H1A \cdots O3 = 153(3)^\circ$; $N1 \cdots O2 = 2.7967(9) \text{ \AA}$, $N1-H1C \cdots O2 = 1.89(3) \text{ \AA}$, $\angle N1-H1C \cdots O2 = 177(3)^\circ$).

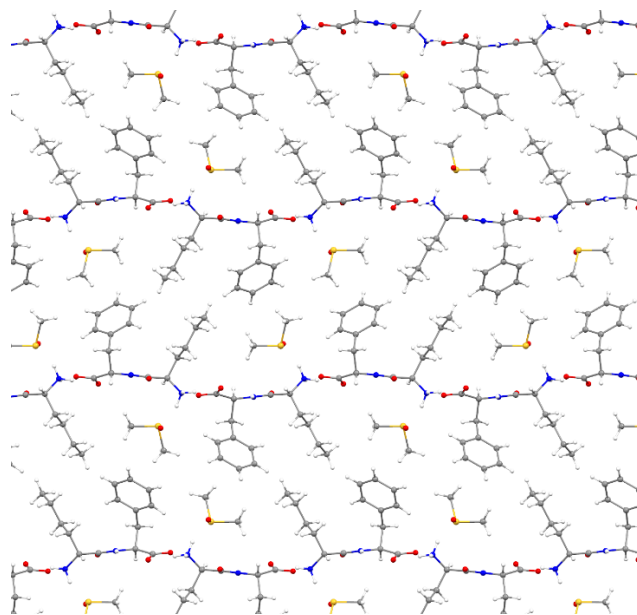


Figure 6. Crystal packing of **2** (view along the *c* axis). Atom types: C gray, H white, O red, N blue, S yellow.

XRD analyses were then performed on xerogels to verify whether a similar packing mode could be found in the gel and crystal phases (Fig. 7 and ESI Section S10). Compound **1** displayed strikingly similar patterns in the two phases that were reminiscent of those displayed by Phe-Phe xerogels and crystals,²⁴ which also assembled in a similar fashion giving rise to water channels whose cavity was defined by 6 peptide molecules arranged head-to-tail. By contrast, the calculated X-ray powder diffraction (XRPD) pattern from single crystal data of **3** was different from the experimental XRPD pattern of the corresponding xerogel, which, instead, was similar to that of compound **1**. We hypothesize that the water channels defined by 4 peptide molecules of **3** found in the crystal structure are not representative of the packing mode in the gel phase that, instead, could display water channels defined by 6 peptide molecules similar to **1**, and to Phe-Phe.²⁴ Analogous was the case for compounds **2** and **4**, whose calculated patterns in the crystal phase were remarkably different from those of the other compounds, and from the experimental pattern

of the xerogel of **2**, which, again, showed similarities with that of **1**. It is possible that in the hydrated gels, compounds **1-3** pack similarly to form water channels defined by 6 peptide molecules, as supported by similar Raman spectra too. It is worth noting that D-Phe-L-Phe, which displays a similar packing mode, was found to form nanotubes defined by two peptide layers and with an outer diameter of 4.3 nm,²⁴ which matches the TEM measurements for individual fibrils of compounds **1-4** shown in Figure 1. Unfortunately, it was not possible to collect the XRPD pattern of **4**, which inevitably crystallized under self-assembly conditions, analogously to D-Phe-L-Leu.²⁸

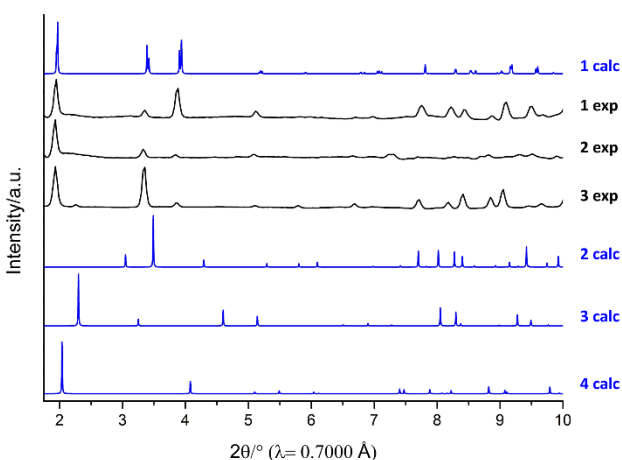


Figure 7. Calculated (calc., blue) and experimental (exp., black) XRPD patterns of **1**, **2**, **3** and **4**.

Conformational analysis

The four dipeptides were analyzed for their conformation by circular dichroism (CD, Fig. 8A). In diluted solutions, the CD spectra of **1** and **2** were similar and displayed two positive maxima at 197 and 212-217 nm. The CD spectrum of **3** displayed less intense maxima at 198 and 220 nm. Conversely, peptide **4** was the only one with two negative minima at 199 and 217 nm. These features were reminiscent of those of similar self-assembling dipeptides that are represented by populations of conformers in solutions,³⁶ and they confirmed that the presence of D-Phe resulted

in negative spectra typical of sequences with D-amino acids, while the presence of L-Phe results in positive spectra in this region. Unfortunately, the formation of opaque gels impeded the acquisition of CD spectra in the assembled states, which were thus analyzed by attenuated total reflectance Fourier-transformed infrared spectroscopy (ATR-IR). In particular, the amide region of the spectra of the xerogels formed by **1** and **3** were strikingly similar (Fig. 8B, left panels), in agreement with the Raman and XRPD data. The amide I signals occurred in the range of β -structures (1610-1622 cm^{-1}) as well as in the range where β -turns are found for longer sequences (1676-1686 cm^{-1}),³⁷ as previously found for the gelling D-Phe-L-Ile, which also formed water channels whose cavity was defined by 6 peptide molecules.³⁸ Peptides **2** and **4** displayed the typical signal at 1641 cm^{-1} too, which is associated with disordered structures.

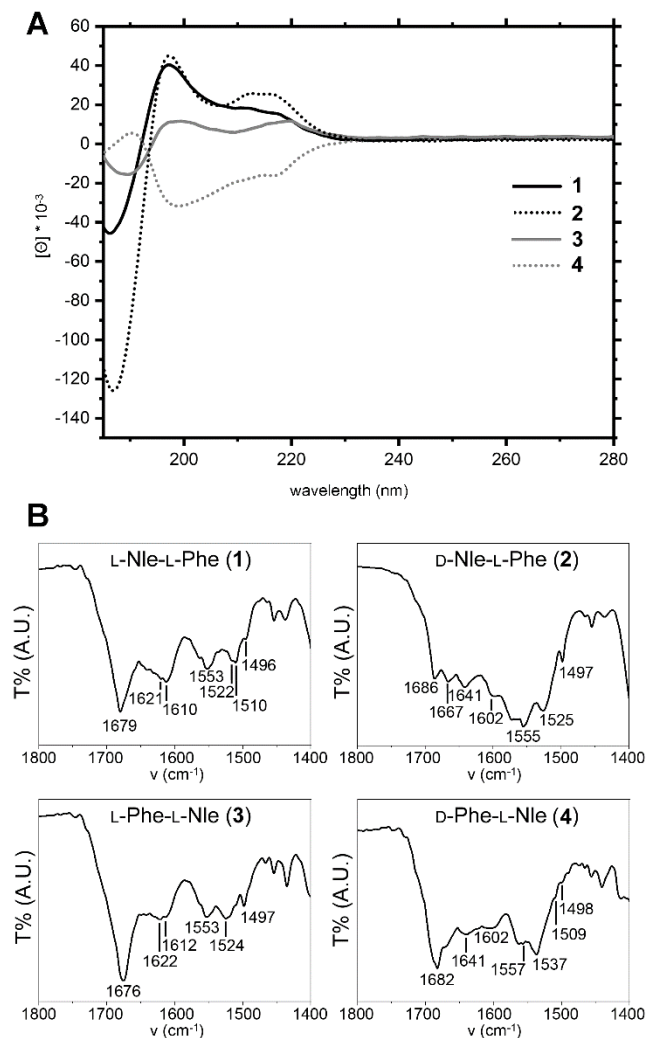


Figure 8. A) CD spectra of compounds **1-4** (1 mM, pH 7). B) ATR-IR spectra of xerogels of compounds **1-4**.

Cell culture

Both hydrogels and solutions of compounds **1-3** were then tested in cell culture for their cytocompatibility. Despite the presence of non-natural Nle, which, in the case of peptide **2**, presented the non-proteogenic D-stereoconfiguration, no signs of cytotoxicity were found. Live/dead assays (Fig. 9) revealed in all cases high numbers of proliferating cells, which grew into the gel reaching the bottom of the microscopy slide, and spread onto its surface. Cellular metabolic

activity was assayed too, using the popular 3-(4,5-dimethylthiazol-2-yl)-2,5-diphenyltetrazolium bromide (MTT) assay (see ESI Section S11).²⁵ Fibroblast cells displayed analogous metabolic activity for the samples that were untreated and served as controls, relative to those that were treated with serial dilutions of peptides **1-3** (1.00 mM – 62.5 μ M).

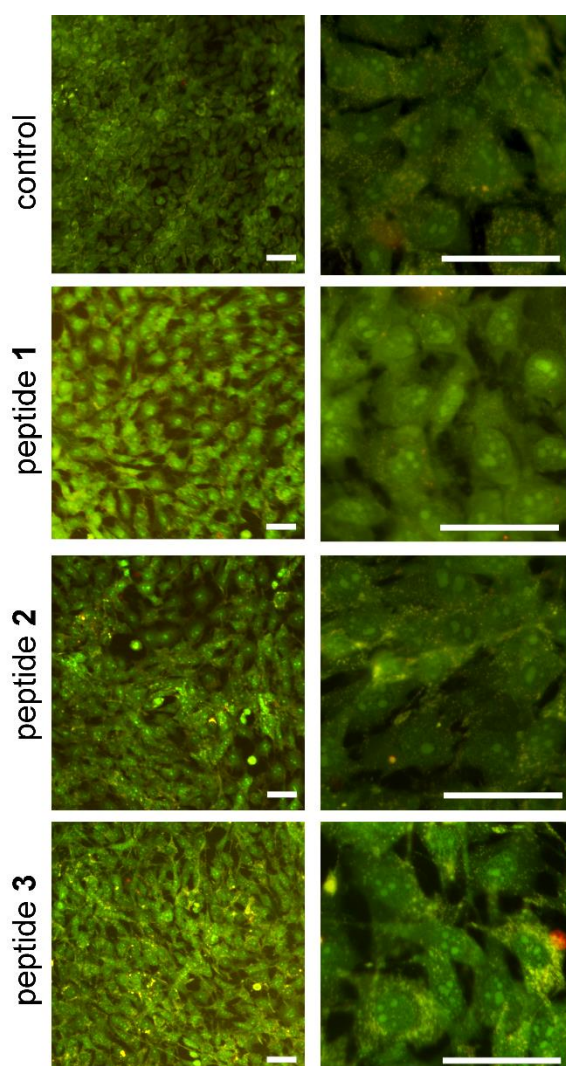


Figure 9. Live/dead assays on fibroblast cells grown without (control) or with peptide **1-3** hydrogels for 24 hours. Scalebar = 50 microns.

Conclusions

This work investigated the supramolecular behavior of dipeptide isomers containing Nle and Phe. All dipeptides **1-4** displayed the ability to self-organize into fibrillar hydrogels in physiologically compatible conditions (PBS, pH 7.3), although those of peptide **4** displayed a metastable character, as they converted into crystals, similarly to D-Phe-L-Leu analogue. All the hydrogels were thermoreversible and displayed good cytocompatibility on fibroblast cells *in vitro*.

Importantly, this work provided the first example of dipeptides that can self-organize into water-channels of differing diameter simply by inverting the amino acid order along the sequence. It also showed that substituting Leu with Nle led to improved gelling ability and lower mgc, confirming the higher ability to pack of the linear side chain of Nle relative to its regioisomers.^{28, 38} In the future, it will be interesting to probe the ability to derivatize these water channels to enable selective transport of small molecules in their interior for a variety of applications.

ASSOCIATED CONTENT

Supporting Information. Spectroscopic, crystallographic, fluorescence, and rheological data are available, as well as the thermoreversibility and MTT tests data, and crystallographic details. The following files are available free of charge.

Supplementary Material (PDF)

crystallographic data (cif, checkcif)

AUTHOR INFORMATION

Corresponding Author

*ctedesco@unisa.it, smarchesan@units.it

Author Contributions

The manuscript was written through contributions of all authors. All authors have given approval to the final version of the manuscript.

Funding Sources

The authors acknowledge funding from the University of Trieste (FRA2023 to S.M.), from the Italian Ministry of University and Research through the PRIN2022 program (SHAZAM project to S.M., grant n. 2022XEZK7K) and the Slovenian Research and Innovation Agency (ARIS: P2-0089, J2-3043, J2-3040, J2-3046, J3-3079, J7-4420 and bilateral ARIS projects BI-FR/23-24-PROTEUS-005 and BI-RS/23-25-030 to S.K.), and the CENN Nanocenter for TEM access.

ACKNOWLEDGMENT

We gratefully acknowledge Elettra Sincrotrone Trieste for providing access to its synchrotron radiation facilities and for financial support (proposal number 20210482).

REFERENCES

1. Lau, H. K.; Kiick, K. L., Opportunities for Multicomponent Hybrid Hydrogels in Biomedical Applications. *Biomacromolecules* **2015**, *16* (1), 28-42.
2. Custódio, C. A.; Reis, R. L.; Mano, J. F., Photo-Cross-Linked Laminarin-Based Hydrogels for Biomedical Applications. *Biomacromolecules* **2016**, *17* (5), 1602-1609.
3. Clapacs, Z.; Oneill, C. L.; Shrimali, P.; Lokhande, G.; Files, M.; Kim, D. D.; Gaharwar, A. K.; Rudra, J. S., Coiled Coil Crosslinked Alginate Hydrogels Dampen Macrophage-Driven Inflammation. *Biomacromolecules* **2022**, *23* (3), 1183-1194.
4. Oliveira, M. B.; Bastos, H. X. S.; Mano, J. F., Sequentially Moldable and Bondable Four-Dimensional Hydrogels Compatible with Cell Encapsulation. *Biomacromolecules* **2018**, *19* (7), 2742-2749.
5. Das, P.; Heuser, T.; Wolf, A.; Zhu, B.; Demco, D. E.; Ifuku, S.; Walther, A., Tough and Catalytically Active Hybrid Biofibers Wet-Spun From Nanochitin Hydrogels. *Biomacromolecules* **2012**, *13* (12), 4205-4212.
6. Truong, V. X.; Tsang, K. M.; Simon, G. P.; Boyd, R. L.; Evans, R. A.; Thissen, H.; Forsythe, J. S., Photodegradable Gelatin-Based Hydrogels Prepared by Bioorthogonal Click Chemistry for Cell Encapsulation and Release. *Biomacromolecules* **2015**, *16* (7), 2246-2253.
7. Truong, V. X.; Tsang, K. M.; Forsythe, J. S., Nonswelling Click-Cross-Linked Gelatin and PEG Hydrogels with Tunable Properties Using Pluronic Linkers. *Biomacromolecules* **2017**, *18* (3), 757-766.

8. Guo, R.; Sinha, N. J.; Misra, R.; Tang, Y.; Langenstein, M.; Kim, K.; Fagan, J. A.; Kloxin, C. J.; Jensen, G.; Pochan, D. J.; Saven, J. G., Computational Design of Homotetrameric Peptide Bundle Variants Spanning a Wide Range of Charge States. *Biomacromolecules* **2022**, *23* (4), 1652-1661.
9. Ghosh, M.; Majkowska, A.; Mirsa, R.; Bera, S.; Rodríguez-Cabello, J. C.; Mata, A.; Adler-Abramovich, L., Disordered Protein Stabilization by Co-Assembly of Short Peptides Enables Formation of Robust Membranes. *ACS Appl. Materials & Interfaces* **2022**, *14* (1), 464-473.
10. Nandi, N.; Gayen, K.; Ghosh, S.; Bhunia, D.; Kirkham, S.; Sen, S. K.; Ghosh, S.; Hamley, I. W.; Banerjee, A., Amphiphilic Peptide-Based Supramolecular, Noncytotoxic, Stimuli-Responsive Hydrogels with Antibacterial Activity. *Biomacromolecules* **2017**, *18* (11), 3621-3629.
11. Redondo-Gómez, C.; Abdouni, Y.; Becer, C. R.; Mata, A., Self-Assembling Hydrogels Based on a Complementary Host–Guest Peptide Amphiphile Pair. *Biomacromolecules* **2019**, *20* (6), 2276-2285.
12. Redondo-Gómez, C.; Padilla-Lopátegui, S.; Mata, A.; Azevedo, H. S., Peptide Amphiphile Hydrogels Based on Homoternary Cucurbit[8]uril Host-Guest Complexes. *Bioconjugate Chem.* **2022**, *33* (1), 111-120.
13. Sangji, M. H.; Sai, H.; Chin, S. M.; Lee, S. R.; R Sasselli, I.; Palmer, L. C.; Stupp, S. I., Supramolecular Interactions and Morphology of Self-Assembling Peptide Amphiphile Nanostructures. *Nano Lett.* **2021**, *21* (14), 6146-6155.
14. Ghosh, M.; Halperin-Sternfeld, M.; Grigoriants, I.; Lee, J.; Nam, K. T.; Adler-Abramovich, L., Arginine-Presenting Peptide Hydrogels Decorated with Hydroxyapatite as Biomimetic Scaffolds for Bone Regeneration. *Biomacromolecules* **2017**, *18* (11), 3541-3550.
15. Mañas-Torres, M. C.; Gila-Vilchez, C.; Vazquez-Perez, F. J.; Kuzhir, P.; Momier, D.; Scimeca, J.-C.; Borderie, A.; Goracci, M.; Burel-Vandenbos, F.; Blanco-Elices, C.; Rodriguez, I. A.; Alaminos, M.; de Cienfuegos, L. Á.; Lopez-Lopez, M. T., Injectable Magnetic-Responsive Short-Peptide Supramolecular Hydrogels: Ex Vivo and In Vivo Evaluation. *ACS Appl. Mater. Interfaces* **2021**, *13* (42), 49692-49704.
16. Wychowanec, J. K.; Smith, A. M.; Ligorio, C.; Mykhaylyk, O. O.; Miller, A. F.; Saiani, A., Role of Sheet-Edge Interactions in β -sheet Self-Assembling Peptide Hydrogels. *Biomacromolecules* **2020**, *21* (6), 2285-2297.
17. Elsayy, M. A.; Wychowanec, J. K.; Castillo Díaz, L. A.; Smith, A. M.; Miller, A. F.; Saiani, A., Controlling Doxorubicin Release from a Peptide Hydrogel through Fine-Tuning of Drug–Peptide Fiber Interactions. *Biomacromolecules* **2022**, *23* (6), 2624-2634.
18. Wychowanec, J. K.; Patel, R.; Leach, J.; Mathomes, R.; Chhabria, V.; Patil-Sen, Y.; Hidalgo-Bastida, A.; Forbes, R. T.; Hayes, J. M.; Elsayy, M. A., Aromatic Stacking Facilitated Self-Assembly of Ultrashort Ionic Complementary Peptide Sequence: β -Sheet Nanofibers with Remarkable Gelation and Interfacial Properties. *Biomacromolecules* **2020**, *21* (7), 2670-2680.
19. Alshehri, S.; Susapto, H. H.; Hauser, C. A. E., Scaffolds from Self-Assembling Tetrapeptides Support 3D Spreading, Osteogenic Differentiation, and Angiogenesis of Mesenchymal Stem Cells. *Biomacromolecules* **2021**, *22* (5), 2094-2106.
20. Zaguri, D.; Zimmermann, M. R.; Meisl, G.; Levin, A.; Rencus-Lazar, S.; Knowles, T. P. J.; Gazit, E., Kinetic and Thermodynamic Driving Factors in the Assembly of Phenylalanine-Based Modules. *ACS Nano* **2021**, *15* (11), 18305-18311.

21. Reja, R. M.; Patel, R.; Kumar, V.; Jha, A.; Gopi, H. N., Divergent Supramolecular Gelation of Backbone Modified Short Hybrid δ -Peptides. *Biomacromolecules* **2019**, *20* (3), 1254-1262.
22. Malhotra, K.; Shankar, S.; Rai, R.; Singh, Y., Broad-Spectrum Antibacterial Activity of Proteolytically Stable Self-Assembled $\alpha\gamma$ -Hybrid Peptide Gels. *Biomacromolecules* **2018**, *19* (3), 782-792.
23. Hu, T.; Agazani, O.; Nir, S.; Cohen, M.; Pan, S.; Reches, M., Antiviral Activity of Peptide-Based Assemblies. *ACS Appl. Mater. Interfaces* **2021**, *13* (41), 48469-48477.
24. Kralj, S.; Bellotto, O.; Parisi, E.; Garcia, A. M.; Iglesias, D.; Semeraro, S.; Deganutti, C.; D'Andrea, P.; Vargiu, A. V.; Geremia, S.; De Zorzi, R.; Marchesan, S., Heterochirality and Halogenation Control Phe-Phe Hierarchical Assembly. *ACS Nano* **2020**, *14* (12), 16951-16961.
25. Bellotto, O.; Pierri, G.; Rozhin, P.; Polentarutti, M.; Kralj, S.; D'Andrea, P.; Tedesco, C.; Marchesan, S., Dipeptide self-assembly into water-channels and gel biomaterial. *Org. Biomol. Chemistry* **2022**, *20* (31), 6211-6218.
26. Macrae, C. F.; Sovago, I.; Cottrell, S. J.; Galek, P. T. A.; McCabe, P.; Pidcock, E.; Platings, M.; Shields, G. P.; Stevens, J. S.; Towler, M.; Wood, P. A. Mercury 4.0: from visualization to analysis, design and prediction. *J. Appl. Crystallogr.* **2020**, *53*, 226-235.
27. Hammersley, A. P. FIT2D: An Introduction and Overview. **1997** ESRF Internal Report, ESRF97HA02T.
28. Bellotto, O.; Kralj, S.; De Zorzi, R.; Geremia, S.; Marchesan, S., Supramolecular hydrogels from unprotected dipeptides: a comparative study on stereoisomers and structural isomers. *Soft Matter* **2020**, *16* (44), 10151-10157.
29. Garcia, A. M.; Iglesias, D.; Parisi, E.; Styan, K. E.; Waddington, L. J.; Deganutti, C.; De Zorzi, R.; Grassi, M.; Melchionna, M.; Vargiu, A. V.; Marchesan, S., Chirality Effects on Peptide Self-Assembly Unraveled from Molecules to Materials. *Chem* **2018**, *4* (8), 1862-1876.
30. Scarel, E.; Bellotto, O.; Rozhin, P.; Kralj, S.; Tortora, M.; Vargiu, A. V.; De Zorzi, R.; Rossi, B.; Marchesan, S., Single-atom substitution enables supramolecular diversity from dipeptide building blocks. *Soft Matter* **2022**, *18* (11), 2129-2136.
31. Balakrishnan, G.; Spiro, T. G., Ultraviolet Resonance Raman (UVRM) Spectroscopy Studies of Structure and Dynamics of Proteins. In *Encyclopedia of Biophysics*, Roberts, G. C. K., Ed. Springer Berlin Heidelberg: Berlin, Heidelberg, **2013**; pp 2697-2707.
32. Görbitz, C. H., Nanotube formation by hydrophobic dipeptides. *Chem. Eur. J.* **2001**, *7* (23), 5153-9.
33. Görbitz, C. H., The structure of nanotubes formed by diphenylalanine, the core recognition motif of Alzheimer's beta-amyloid polypeptide. *Chem. Commun.* **2006**, (22), 2332-4.
34. Sawaya, M. R.; Sambashivan, S.; Nelson, R.; Ivanova, M. I.; Sievers, S. A.; Apostol, M. I.; Thompson, M. J.; Balbirnie, M.; Wiltzius, J. J.; McFarlane, H. T.; Madsen, A.; Riek, C.; Eisenberg, D., Atomic structures of amyloid cross-beta spines reveal varied steric zippers. *Nature* **2007**, *447* (7143), 453-457.
35. Marchesan, S.; Waddington, L.; Easton, C. D.; Winkler, D. A.; Goodall, L.; Forsythe, J.; Hartley, P. G., Unzipping the role of chirality in nanoscale self-assembly of tripeptide hydrogels. *Nanoscale* **2012**, *4* (21), 6752-6760.

36. Monti, M.; Scarel, E.; Hassanali, A.; Stener, M.; Marchesan, S., Diverging conformations guide dipeptide self-assembly into crystals or hydrogels. *Chem. Commun.* **2023**, *59* (73), 10948-10951.
37. Goormaghtigh, E.; Ruyschaert, J. M.; Raussens, V., Evaluation of the information content in infrared spectra for protein secondary structure determination. *Biophys. J.* **2006**, *90* (8), 2946-57.
38. Bellotto, O.; Kralj, S.; Melchionna, M.; Pengo, P.; Kisovec, M.; Podobnik, M.; De Zorzi, R.; Marchesan, S., Self-Assembly of Unprotected Dipeptides into Hydrogels: Water-Channels Make the Difference. *ChemBioChem* **2022**, *23* (2), e202100518.